

DOI: 10.1002/elan.201700304

Thin-Film Potentiometric Sensor to Detect CO₂ Concentrations Ranging Between 2 % and 100 %

Lander Rojo,^[b] Irene Castro-Hurtado,^[b] Gemma G. Mandayo,^[b] Enrique Castaño,^[b] and Maria C. Morant-Miñana*^[a]

Abstract: A potentiometric thin-film sensor to detect CO₂ in a wide range (2–100 %) has been developed. The system has been fabricated depositing a reference electrode of Pt, a solid electrolyte of YSZ (Yttria-stabilized Zirconia), a sensing phase made of Li₂CO₃ and a working electrode of Au via Physical Vapor Deposition (PVD). Characterization of the different elements has provided the optimal fabrication parameters and the system response for CO₂ concentrations can be measured from 2 to 100 % at 450 °C. The sensor behaves as a non-Nernstian system and slightly deviates from a linear response with

the logarithm of CO₂ until the CO₂ concentration reaches the 30 %. Higher CO₂ amounts make the response divert more from the Nernst law but give a stable and reproducible response to CO₂ in a wide range of concentrations. Based on these promising results the recovery time, stability, repeatability and selectivity of the sensor have been measured. The performance showed by the thin film sensor proves the feasibility of the use of this system for biogas and natural gas applications owing to its very good consistency at low temperature in a wide concentration range.

Keywords: non-Nernstian · CO₂ · thin-film · YSZ · potentiometric sensor

1 Introduction

■■■Dear Author, please note that we changed the order of the headlines. In Full Papers „Experimental“ usually appears after „Introduction“

Dear author please correct the journalnames in the references!!! They should be abbreviated!!!■■■

The modern society has strong dependence on fossil fuels. Mineral carbon, petrol and natural gas are the main actors of the current industrial, economic and social moment that we are living. However, these resources are limited and contain a huge amount of carbon, released to the atmosphere as CO₂ being one of the main contributors to the green house effect. In order to decrease CO₂ emissions, sustainable energies are being developed. Among others, biogas is a very interesting alternative because it uses the organic wastes generated in farms, plants of residual water and waste disposal sites and exploits the methane generated from its anaerobic digestion (oxygen absence), avoiding the emission of polluting agents to the atmosphere. The quality of the gas is correlated with the amount of CO₂. Usually the CO₂ percentages found in biogas are in the range of 25 % to 55 %. In some plants, biogas is used as another methane source for natural gas production, however to distribute the gas inside the natural gas pipelines the percentage of CO₂ should be reduced to less than 3 % because CO₂ is an inert gas in terms of combustion and decreases the energetic content of the biogas [1]. For this reason wide range CO₂ gas sensors are considered a fundamental tool needed to monitor the quality of the gas concentration in biogas and its use for natural gas production.

To detect gases in a broad detection range, gas chromatography and infrared absorption spectroscopy are the most used techniques. The main problem of these methods is the expensive price of the devices and facilities needed. Hence, researchers worldwide are trying to meet the demand of devices that can be used to monitor the network condition at reduced cost. Recently, Köhring *et al.* [2] have shown the feasibility of a light emitting diode-based quartz enhanced photoacoustic sensor for methane and CO₂ detection in biogas plants with fast response time, broad concentration range and low cross sensitivities. However, the sensor showed temperature and pressure dependent signal variations. Therefore there is still a necessity to develop new sensors that are able to measure CO₂ in a wide detection range with ready confidence.

Electrochemical sensors are an interesting alternative to these methods, since they can transform an electrochemical parameter in an electrical signal. In particular, solid-state sensors use solid electrolytes to monitor the potential of an open circuit between the electrodes. Usually, the electric potential differences (ΔV) are proportional to the logarithm of the analyte concentra-

[a] Dr. M. C. Morant-Miñana
CIC nanoGUNE, Tolosa Hiribidea, 76, 20018 Donostia
E-mail: mc.morant@nanogune.eu

[b] Dr. L. Rojo, Dr. I. Castro-Hurtado, G. G. Mandayo,
E. Castaño
Paseo Manuel Lardizabal, 15, 20018 Donostia

Supporting information for this article is available on the WWW under <https://doi.org/10.1002/elan.201700304>

tion, following the Nernst equation [3]. This kind of sensors are commonly applied for low gas concentrations 0.002 % and 2 % (10–10000 ppm) using the linear region of the logarithmic response to monitor emitted CO₂ on-line with high selectivity, high sensitivity, improved long-term stability and reduced cost [4–5]. On the contrary, few authors have reported the potential of these sensors for detecting high CO₂ concentrations. For instance, Lee *et al.* [6] described a thin-film potentiometric CO₂ sensor based on Li₃PO₄ as solid electrolyte and Li₂CO₃ as sensing electrode. The thin-film sensor (1 μm-thick) had a better sensing response for CO₂ concentrations than the sensor with thick-film electrolyte, showing that thick electrolytes result in devices with longer response time and lesser sensitivity. Moreover, the thickness decrease allowed for measuring CO₂ concentrations ranging between 500 ppm and 20%. However, the existence of potentiometric sensors working over all CO₂ concentrations (up to 100 %) is still a major limitation.

In this paper, a rapid and reliable planar gas sensor using interdigitated electrodes and electrolytes made of thin films (300 nm) has been designed and fabricated. The sensor is based on an YSZ electrolyte (300 nm) and Li₂CO₃ (300 nm) as a sensitive element. The fabrication of these two elements has been performed using magnetron sputtering and supposes one of the first examples of the combination of carbonates and YSZ electrolytes, as a thin-film, for measuring CO₂ in a wide range of concentrations. The structural characterization of the sensor elements and the electric potential differences at concentrations between 2 % and 100 % CO₂ are described. Even at very low temperatures (450 °C), the sensor obeys the mixed potential mechanism with two slopes that describes two different behaviors depending on the concentration. The sensitivity, selectivity and recovery times of the system are also investigated.

2 Experimental

YSZ (Testbourne Zirconia 5 % wt Yttria) and Li₂CO₃ (Testbourne 99.9 %) deposition was performed from a high purity targets by RF magnetron sputtering (Pfeiffer Classic 500). Au and Pt layers were deposited by DC magnetron sputtering (Edwards coating system E306A) and the thermal treatments were performed in an ATV PEO 601 furnace. The thickness values of the sensor fabricated were measured using a mechanical profilometer.

The crystallographic structure of the YSZ films before and after the thermal treatments was analysed by X-ray diffraction (XRD) by means of a Philips XPERT MRD diffractometer in a glancing angle configuration ($\omega = 2^\circ$ and Cu K $\alpha_1 = 1.54059$ Å). The diffraction patterns were obtained in the 20°–80° range with a step size of 0.015° a time per step of 6.5 seconds. Cyclic voltammetry (CV) measurements were performed using a potentiostat from CH Instruments 1000 B. The Electrochemical Impedance Spectroscopy (EIS) analysis was performed with a Solar-

tron 1260 frequency response analyser in the frequency range from 0.1 Hz to 4 MHz and applied amplitude of 200 mV. Afterwards, the obtained impedance patterns were fitted with Zview and Zplot using an equivalent circuit in order to quantitatively analyse the obtained results. The gas response measurements were performed in a controlled gas atmosphere by means of a computer-controlled flow of 200 sccm from Bronkhorst Hi-Tech, using certified bottles of 99.9 % CO₂, O₂, N₂ and CH₄ provided by Air Liquide. The % of CO₂ was diluted from 100 % to 2 % using mass flow controllers. The sensor was welded to a custom-made PCB and mounted in an aluminium chamber (1200 cm³) and heated at the operating temperature via the platinum heater deposited below the substrate. The process was controlled using an internal PC using tailored National Instruments LabView software.

3 Results and Discussion

First of all the influence of the annealing temperature on the crystallization process of the solid electrolyte was studied using XRD onto continuous YSZ films of 100 nm, 200 nm and 300 nm thicknesses. In all cases the obtained Bragg peaks are characteristic of a cubic structure with a (111) preferred orientation (matches the reference pattern ICDD: 00-030-1468) in accordance with the literature [7–9]. An average grain size of 14.9 nm and a lattice parameter of around 5.1390 Å were measured using the Scherrer formula. Observing the intensity of the peaks, a change of the (111) peak with the annealing temperature can be noticed. The annealing temperatures (500, 700 and 900 °C) were selected taking into account the phase evolution of the YSZ, the power consumption and the stability of the materials. In this particular case, the annealing temperature of 900 °C has been selected as the optimum since it results in samples with higher crystallinity and the cubic structure.

The YSZ, as ionic conductor, has been thoroughly studied by electrochemical methods such as EIS [10]. This technique allows studying the influence of the microstructure on the ionic conductivity of the material and can determine the optimal thickness of the electrolyte. EIS analysis was carried out on samples of different thickness annealed at 900 °C in a synthetic air atmosphere in a measuring range from 200 °C to 450 °C. To characterize optimal operating temperature of the solid electrolyte (YSZ), a 200 nm-thick Pt interdigitated electrodes with a finger width of 25 μm were deposited on the top part of the Al₂O₃ substrate. On the back of the Al₂O₃ substrate a 200 nm-thick Pt heater was deposited to heat the system. A representative example of the impedance pattern of samples of 100 nm, 200 nm and 300 nm measured at 450 °C can be seen in the SI (Supporting Information). The impedance spectrum shows a graph that consists of two arcs. The high frequency arc (left hand arc) corresponds to the processes involved in the conduction through the YSZ electrolyte, this is, the conduction

through the grain and along the grain boundaries. The low frequency arc (right hand arc) represents the reaction that takes place in the electrodes. The spectra were analyzed with the equivalent circuit showed in the SI and the R_s (resistance of the connections) and $R_{p||Cp}$ (conduction through the YSZ electrolyte) values were determined. The dependency of the resistance with the temperature was plotted and the Arrhenius graphs (see SI) were obtained and used to analyze quantitatively the evolution of the activation energy with the thickness. The samples of 100 nm, 200 nm and 300 nm had activation energies of 1.18 ± 0.02 eV, 1.11 ± 0.01 eV and 0.99 ± 0.01 eV, respectively. From these data, it can be concluded that the activation energy decreases with the YSZ thickness. Lower activation energy values have been obtained for 300 nm thick samples annealed at 900°C for 2 hours. These values are in agreement with the values calculated for different authors [11]. Once the operating parameters of the electrolyte were established, the ionic conductivity was calculated from the Nyquist impedance probe using the equation (1):

$$s = L / (R \cdot W \cdot t) \quad (1)$$

where L is the distance between the Pt electrodes ($25 \mu\text{m}$), t the thickness of the coating and W the width of the electrolyte [12]. Values of 1.02×10^{-8} , 3.85×10^{-8} and $1.39 \times 10^{-7} \text{Scm}^{-1}$ were calculated for the samples of 300 nm measured at 315°C , 345°C and 415°C , respectively. Comparison of the ionic conductivities of the 5 mol% YSZ with the values found in the literature (see SI) is difficult since these values depend on the processing method and the microstructure. However our results confirm that annealing the 300 nm-thick of YSZ films at 900°C make this electrolyte suitable for the use in a potentiometric sensor due to the good compromise between the crystallinity, the lower activation energy and the higher ionic mobility.

In the $\text{O}_2(\text{g})/\text{Pt}/\text{YSZ}$ system, various interfaces exist where electrochemical reactions may take place: three binary interfaces (Pt/YSZ , $\text{YSZ}/\text{O}_2(\text{g})$ and $\text{Pt}/\text{O}_2(\text{g})$) and one triple phase boundary (TPB) where the three binary interfaces meet [13]. Since YSZ plays a fundamental role in the working principle of this kind of cell in electrochemical devices, CV measurements have been performed in order to analyze the role of the TPB. Figure 1 shows the different voltammograms obtained in the operating temperature range between 250°C and 450°C . At low temperatures, the exchange current is very small so the reaction from the TPB is not electrocatalytically active. The typical cathodic and anodic peaks start to be visible at 300°C . The anodic peak appears at 2.15V and the cathodic at -2.25V . The formation of these peaks means that the reaction occurs through the TPB and catalyzes the charge transfer reaction. At 300°C the exchange current is larger than before so practically all the oxygen molecules react from the TPB. The area of the peaks is similar ($2.42/2.39 = 1.01$), so the oxygen absorption at the

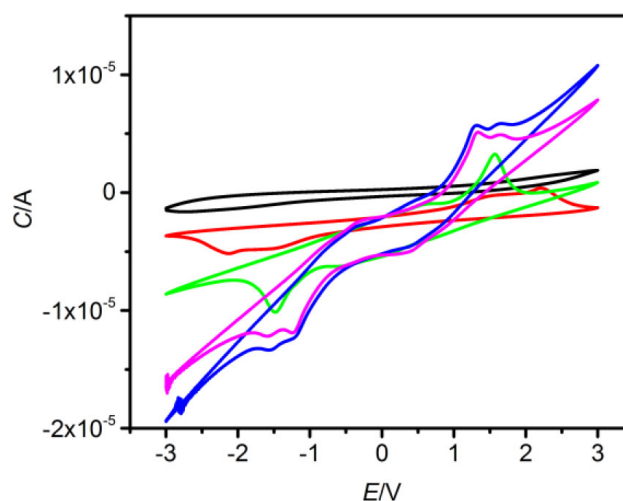


Fig. 1. Cyclic voltammograms of Pt|YSZ cell obtained at (—, black) 250°C , (—, red) 300°C , (—, green) 350°C , (—, pink) 400°C and (—, blue) 450°C at 0.1V/s scan rate.

TPB is less efficient than the charge transfer reaction. The increase of the temperature shows two specific features. The first one is the increase of the peak size until a maximum is reached at 450°C and the second one a gradual approach between the cathodic and the anodic peak. As can be concluded, both processes are highly temperature dependent. Physically, this can be attributed to the increase in exchange current with the temperature. The rise in the reaction temperature accelerates the charge transfer reaction and the reaction becomes more reversible by shifting the peak potential closer to its equilibrium location. It can be observed that two overlapping peaks appear providing strong evidence for the coexistence of two different surface oxygen species as discussed by some authors [14, 15].

Focusing on the tilt presented by the voltammograms, it increases with the operating temperature. This phenomenon can be determined using the Ohm's law. The reactions that take place in the TPB are generally represented by a charge transfer resistance (R_{ct}) that corresponds to the opposition of the system to this reaction and a double layer capacitance (C_{dl}) that represents the potential difference created in the interface [10]. As R_{ct} depends on temperature, an increase of the tilt of the voltammogram represents a decrease in the R_{ct} value due to the temperature. This is in accordance with the EIS measurement where R_{ct} values of $2.45 \times 10^6 \text{ Ohms}$ and $1.80 \times 10^5 \text{ Ohms}$ were obtained for 315°C and 415°C , respectively.

On the other hand, C_{dl} is responsible of the hysteresis (ΔI) observed in the voltammograms and it is proportional to $\delta I / 2\nu$, where δI is the width of the voltammograms and ν the scan rate. In this particular case, the hysteresis increases with the temperature until 450°C where it reaches saturation. This can be explained because at low temperatures, the oxidation process is not fast

enough to avoid the hysteresis at reduction currents. At 450 °C the system is reaching the equilibrium temperature so this process is slowed and will disappear at higher temperatures [16,17].

Various scan rates have been used to determine the length of the TPB (see SI). As the general CV theory explains [18], increasing sweep rate (v) produces a linear increase in the intensity of both peaks and shifts the potentials closer indicating that the process is becoming more reversible. According to Vayenas *et al.* [15] the slope of I_p vs. v can be used for the determination of the amount of electrocatalytically active oxygen in the vicinity of the TPB of YSZ/Pd/O ($N_{0,TPB} = 2.2 \times 10^{-11}$ g-atom O). Taking into account the surface diffusion rate of O on Pt electrodes (4×10^{-11} cm²/s) during a measurement time of 50 s an estimation of a TPB length of 1.3 μ m was determined for our system.

Once the optimal annealing temperature of the electrolyte was maximized, the role of the thickness established and the operating temperature of the electrolyte selected, the fabrication process was performed and it is schematically summarized in Figure 2. Polished Al₂O₃ wafers were used as substrates of the sensors. Prior to the deposition, the substrates were immersed in acetone, ethanol and deionized water and washed for 10 minutes in an ultrasonic bath. YSZ was used as electrolyte and was deposited onto the substrate in Ar atmosphere. The layer was patterned as a square of 1.5 mm \times 1.5 mm and with a 300 nm thickness and a surface roughness of 5 nm (step 1). The as-deposited YSZ films were annealed at 900 °C during two hours (step 2). A 200 nm-thick Pt reference

interdigitated electrode (RE) and a 200 nm Au sensing interdigitated electrode (SE) with 50 μ m of interdigitated space were deposited to have a fine contact with the electrolyte (step 3 and 4). All the metallic layers were annealed at 600 °C during two hours (step 5). Finally, the deposition of the auxiliary phase (AP) of 300 nm of Li₂CO₃ (step 6) was performed as described in previous works [19,20]. The auxiliary phase (AP) was patterned by photolithographic techniques in an interdigitated shape to maximize the contact area among AP, the electrolyte and the SE. Afterwards, the layer was subjected to an annealing treatment of 600 °C during two hours in a CO₂ atmosphere (step 7). On the backside of the Al₂O₃ substrate a metallic layer of 200 nm thick of Pt was deposited (step 8). It is important to point that the only role of the metallic layer deposited in the step 8 is to act as heater of the sensor and does not have any other function in the sensing process. Figure 3 shows the sensor unit. The picture gives an overview of the gas chamber and the connection between the electrode and the electronics unit.

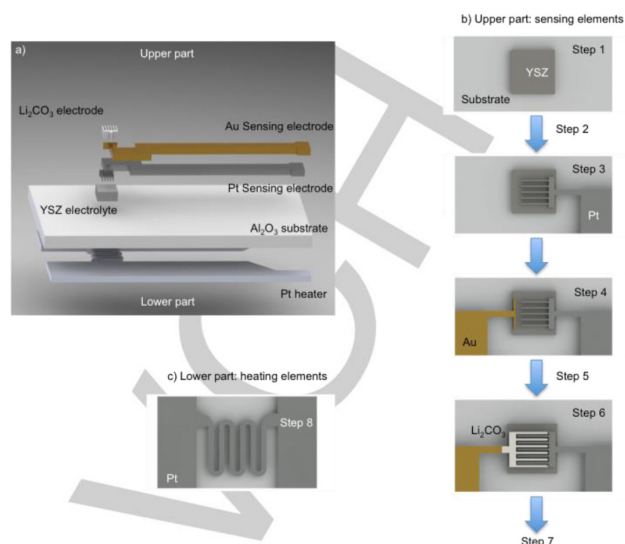


Fig. 2. (a) Schematic view of the planar gas sensor and (b) fabrication steps of the upper part of the CO₂ sensor: (step 1) YSZ deposition; (step 2) thermal treatment of YSZ; (step 3) Pt electrode deposition; (step 4) Au sensing electrode deposition; (step 5) TT of Pt and Au; (step 6) Li₂CO₃ auxiliary electrode deposition; (step 7) thermal treatment of Li₂CO₃. (c) Fabrication steps of the lower part of the CO₂ sensor: (step 8) Pt heater deposition.

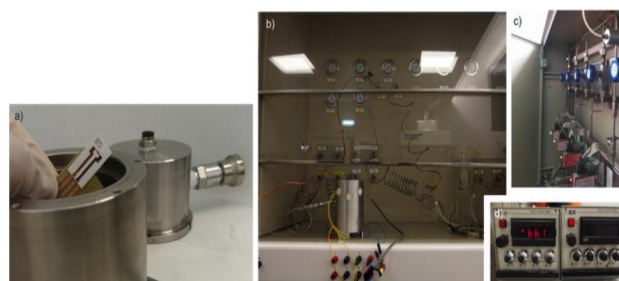


Fig. 3. (a) Sensor and (b) gas chamber showing the integration of the sensor; (c) mass flow controllers and (d) measurement units.

The cross-section of the sensor surface can be viewed in the SI. As can be seen a thickness of 300 nm, 200 nm and 300 nm was measured for YSZ, Au and Li₂CO₃, respectively. For the gas sensor measurement, it was introduced in a chamber and heated via the platinum heater located on the backside of the Al₂O₃ substrate until the desired operating temperature was achieved. The sensing signal of the device is obtained by measuring the ΔV between the sensing electrode (SE) and the reference electrode (RE) against different amounts of CO₂ using CH₄ as a carrier gas. CH₄ was selected as a carrier gas because it is the major compound present in biogas and natural gas. Figure 4a shows representative measurements obtained at 450 °C. The sensor is sensitive to percentages of CO₂ from 2 to 90 % under the tested conditions and the response increases with the CO₂ concentration. For a single measurement, it can be observed that when the sensor is exposed to CO₂ stimuli a ΔV -overshoot at the initial period of each platform is observed. After that, a saturation point is reached and the ΔV response is perfectly stable. This phenomenon can be ascribed to the

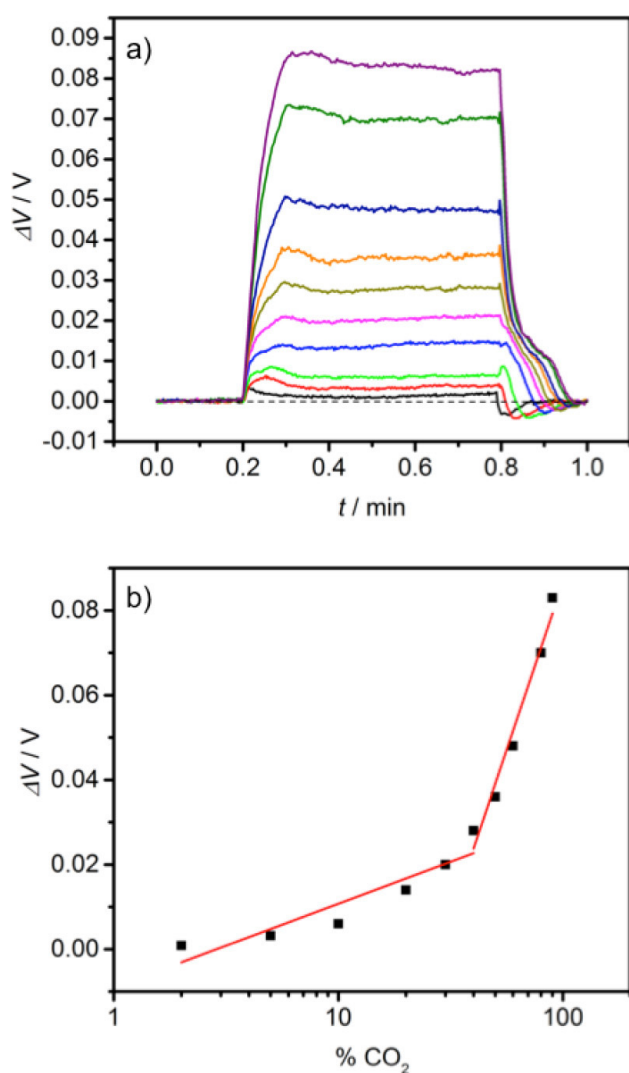
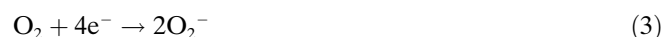


Fig. 4. (a) Electric potential difference of the sensor at 450 °C for various CO₂ concentrations: (–, black) 2%, (–, red) 5%, (–, bright green) 10%, (–, bright blue) 20%, (–, pink) 30%, (–, brown) 40%, (–, orange) 50%, (–, dark blue) 60%, (–, dark green) 80% and (–, purple) 90%. The dotted line shows the values expected for 0% of CO₂. (b) Normalized electric potential difference as a function of the % of CO₂ of the sensor at 450 °C.

heat-inertia of the heater as has been observed for similar systems [21]. Once the stimulus is cut, the sensor recovers the baseline showing a completely reversible behavior. The spikes produced after switching off the gas are artifacts related to the gas dosage system of the test bench. As can be seen at low concentrations, there is no noise in the measurement, the signal is stable without fluctuation and is maintained above 0 during the measurement time. Also, the exposition of the sensor to high CO₂ amounts (over 9 times) showed no change in its response characteristics. It is interesting to point out that the sensor signal has linear dependence with the concentration. This abnormal phenomenon of the potential signal is known as non-Nernstian behavior and is used to describe systems that do not obey the Nernst equation.

The sensing mechanism is based on the mixed potential theory [22]. The theory explains that before the addition of the sample gas (CO₂) both RE and SE electrodes are exposed to CH₄ (reference gas) and the ΔV between both electrodes gives a base signal for the sensor. When the sample gas diluted with the reference gas is introduced, different oxidation (equation 2) and reduction (equation 3) reactions in the SE and the RE led to a steady state in which the electrons from the oxidation reaction are consumed for the reduction generating a potential. In our case this produces an increase in the overpotentials, resulting in a generation of a positive voltage for the sensor.



The ΔV response at 450 °C has been analyzed in detail in Figure 4b. This graph consists of a line with two slopes, which describes two different behaviors of the sensor depending on the concentration: the low concentration region and the high concentration region. As can be seen in the plot, the sensor behaves as a non-Nernstian sensor in the whole range of concentrations based on the low linearity of ΔV with the logarithm of the CO₂ concentrations. The fittings of the values at low (2–30%) and high (>30%) CO₂ concentrations are listed in Table 1.

Table 1. Operating parameters measured for the sensors at 450 °C.

Linear Range ^[a]	Slope ^[b]	n ^[c]	r ^[d]	Sensitivity ^[e]
2–30	0.025	2.4	0.93	4.88
30–100	0.157	0.39	0.99	3.93

[a] % CO₂. [b] (V/dec). [c] R = 8.31 J/Kmol; T = 723.15 K; F = 96500 J/mol. [d] Correlation Coefficient. [e] % CO₂/V cm².

For low concentrations (2–30%), the number of electrons involved in the process (n) was 2.4 and a largest deviation from this behavior was found at higher concentrations. For both ranges the sensor shows a linear relationship that will make the practical application of the system feasible. For this linear range the sensitivity (s) was calculated using $s = m/A$ where m is the slope of the linear equation and A is the area of the electrodes ($A = 0.04 \text{ cm}^2$). Finally, the inflexion point for both lines was calculated for 40.53% of CO₂.

For Nernstian sensors values of 50 mV/dec, 77.9 mV/dec and 90 mV/dec have been found in the literature for CO₂ concentrations ranging between 0.002% and 2%. A very low value of measured sensitivity (25 mV/dec) is reported here although higher concentrations were used (2–30%). A plausible explanation can be the use of thin-films (200–300 nm) as sensing elements increases the performance (sensitivity) of the device toward a wide CO₂ ranges at low temperature. There are only few examples

of potentiometric sensors used for detecting a wide range of CO₂ concentrations. In this context Choi *et al.* have developed a stacked-type potentiometric CO₂ gas sensor to reduce its active area [23]. It shows a very fast response and recovery time at 500 °C compared to planar sensors. However in this system concentrations of CO₂ up to 50 % have been measured. Similar concentrations have been tested with the Bi₈Nb₂O₁₇ and Pt as solid-reference electrode materials for the NASICON-based potentiometric sensor. The system does not deviate from the Nernst equation but detection above 60 % of CO₂ is not reached [21]. CO₂ concentrations between 6 ppm and 100 % have been measured using a compact CO₂ sensor that combines two sodium ionic conductors. The measured response was rapid, continuous, stable, reproducible and independent of P_{O₂} in the gas [24]. In our sensor, the ionic conductivity governs the sensing characteristics of the system.

After establishing the operating parameters, the gas response characteristics were set. The sensor was preheated at 450 °C and stabilized during 10 h to measure the response and the recovery time. The response time (t_{90}) is the time needed to reach the 90 % of its maximum response and the recovery time (t_{rec}) is the reverse. The calculated values for the sensor at 450 °C were 2 and 7 min for t_{90} and t_{rec} , respectively. In general, the sensor shows a sharp response transient for the t_{90} and a lower decay for the t_{rec} due to the high gas volume of the reaction chamber. The values found in the literature for potentiometric sensors using carbonates as sensing electrodes are lower than the values measured for our system. Lee *et al.* measured a t_{90} of 1 min for a sensor made of Li₃PO₄ [6], Kida published a sensor with an electrolyte of NASICON and reported a t_{90} of 20 s [25], Park reported a sensor with an electrolyte of Li₂PO₄ with t_{90} = 30 s and Choi published a sensor made of Li₃PO₄ with a t_{90} of 2 s and t_{rec} of 4 s [23]. The absence of information regarding the chamber volume and gas flows in these papers difficulties the comparison of the results. Moreover, it is important to point that these systems operate at different temperatures (higher than 450 °C) and this fact can lower the response kinetics.

In general, the stability of the sensor is a very important parameter because its lifetime should be at least from 2 to 3 years [26]. Thermal stability is a parameter that will affect directly the potential use of the sensor. The thermal stability of the sensor measured at 400 °C during 5 days is shown in the SI. The measurement corresponds to the values of the baseline reached after measuring the signal repeatedly with a 70 % of CO₂. The sensor shows a stable baseline with an increasing upward shift with time. From this experiment it can be concluded that the mild temperatures selected for the system, are preferable and result in a stable interface between the electrolytes and the electrodes. This experiment was also suitable to study the repeatability of the system. The variation coefficient obtained after different measurements in the described period of time obtained was 7 %.

This means that the repeatability of the sensor is good and the response is stable during the tested period.

Selectivity is a basic parameter to characterize the analytical properties of a sensor because other gases can cause variations of the signal sensor response. In the case of sensors for biogas applications, N₂ and oxygen can act as interfering of the measurements. To test the selectivity of our sensor, it was exposed to usual percentages of N₂ and oxygen that can be found in biogas mixtures together with CO₂.

Figure 5 shows the response of the sensor to 40 % (SEN2) and 60 % (SEN1) of CO₂ concentrations as negative controls. As can be seen in the figure, addition of 2.5 % (SEN3) or 5 % (SEN4) of N₂ in an atmosphere with CO₂ has little influence on the sensor and only small differences can be measured from the background. In particular a 0.96 % and 1.24 % deviation of the signal was measured for N₂ concentrations of 2.5 % and 5 %, respectively. In the case of the oxygen (SEN5) a deviation from the CO₂ response shows a dependency of the sensor with the coexistent O₂ concentration. In particular the deviation of the signal obtained after the introduction of N₂, O₂ and CO₂ gases (SEN6) is 10% higher than the signal measured for CO₂ alone (SEN2). A plausible explanation of the sensor behavior against oxygen can be the different reactions occurring at the electrodes. As a result different catalytic activities could influence various competing processes. Based on these results we can affirm that the fabricated sensor showed a good performance in sensing CO₂ gas but also has small response to O₂ as interfering gas.

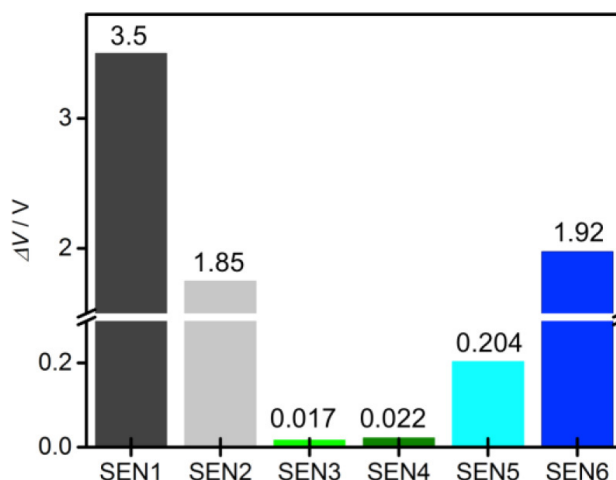


Fig. 5. Electric potential difference of the sensor at 60 % (SEN1) and 40 % (SEN2) of CO₂ and selectivity of the CO₂ sensor against 2.5 % of N₂ (SEN3), 5 % of N₂ (SEN4) and 5 % of O₂ (SEN5) as interfering gases. Electric potential difference of the sensor (SEN6) against a mixture of CO₂, N₂ and O₂. A bar break has been included in SEN1, SEN2 and SEN6 to better disclose the results.

4 Conclusions

In this work, a planar potentiometric sensor that consists of Au and Pt interdigitated electrodes has been fabricated. The sensor design is based on interfacing electrolytes of less than 300 nm thick. YSZ and Li_2CO_3 have been used as solid electrolyte and sensing phase, respectively. The ΔV of the sensor shows a non-Nernstian behavior in the whole range of concentrations with two slopes depending on the concentration. The operating temperature of the system has been selected at 450 °C, which is one of the lowest operating temperatures reported in the literature for similar sensors. A stable and reproducible response presented by the sensor has been demonstrated, however some issues can be improved related to the selectivity of the sensor that will be addressed in the forthcoming developments. Substantially smaller size, lower mass, lower power requirements, greater sensitivity, and better specificity are the potential benefits of exploiting microelectronics and nanotechnology in sensor fabrication. All the experimental results show that this miniaturized sensor can be used as diagnostic tool for identifying wide range and high CO_2 concentrations and is suitable for monitoring the quality of the wide CO_2 concentrations required in biogas and natural gas production.

Acknowledgements

MC M-M acknowledges the Basque Government under the Etortek Program (Grant No. IE14-391) and Dr Seifert for the use of his facilities.

References

- [1] N. Abatzoglou, S. Boivin, *Biofuels Bioproducts and Biorefining* **2009**, *3*, 42–71.
- [2] M. Köhring, S. Böttger, U. Willer, W. Schade, *Sensors* **2015**, *15*, 12092.
- [3] P. Pasierb, M. Rekas, *Journal of Solid State Electrochemistry* **2009**, *13*, 3–25.
- [4] T. Okamoto, Y. Shimamoto, N. Tsumura, Y. Itagaki, H. Aono, Y. Sadaoka, *Sensors and Actuators B Chemical* **2005**, *108*, 346–351.
- [5] Y. Shimamoto, T. Okamoto, Y. Itagaki, H. Aono, Y. Sadaoka, *Sensors and Actuators B Chemical* **2004**, *99*, 113–117.
- [6] I. Lee, S. A. Akbar, *Ionics* **2014**, *20*, 563–569.
- [7] N. H. Perry, S. Kim, T. O. Mason, *Journal of Materials Science* **2008**, *43*, 4684–4692.
- [8] F. Smeacetto, M. Salvo, L. C. Ajitdoss, S. Perero, T. Moskalewicz, S. Boldrini, L. Doubova, M. Ferraris, *Materials Letters* **2010**, *64*, 2450–2453.
- [9] W. Zhao, I. J. Kim, J. Gong, *Journal of the Ceramic Society of Japan* **2010**, *118*, 550–554.
- [10] J. E. Bauerle, *Journal of Physics and Chemistry of Solids* **1969**, *30*, 2657–2670.
- [11] J. Jiang, X. Hu, N. Ye, J. L. Hertz, *Journal of the American Ceramic Society* **2014**, *97*, 1131–1136.
- [12] J. F. Vélez, R. A. Procaccini, M. Aparicio, J. Mosa, *Electrochim. Acta* **2013**, *110*, 200–207.
- [13] A. Jaccoud, G. Fóti, R. Wüthrich, H. Jotterand, C. Comninellis, *Topics in Catalysis* **2007**, *44*, 409–417.
- [14] H. Pöpke, E. Mutoro, B. Luerßen, J. Janek, *Catalysis Today* **2013**, *202*, 12–19.
- [15] C. G. Vayenas, A. Ioannides, S. Bebelis, *Journal of Catalysis* **1991**, *129*, 67–87.
- [16] M. W. Breiter, K. Leeb, G. Fafilek, *Electrochim. Acta* **1998**, *43*, 325–334.
- [17] H. Y. Lee, W. S. Cho, S. M. Oh, H. D. Wiemhöfer, W. Göpel, *Journal of The Electrochemical Society* **1995**, *142*, 2659–2664.
- [18] A. J. Bard, L. R. Faulkner, *Electrochemical Methods Fundamentals and Applications*, 2nd Edition ed., John Wiley and Sons, New York, **2001**.
- [19] L. Rojo, I. Castro-Hurtado, M. C. Morant-Minana, G. G. Mandayo, E. Castano, *CrystEngComm* **2014**, *16*, 6033–6038.
- [20] L. Rojo, I. Castro-Hurtado, M. C. Morant-Minana, G. G. Mandayo, E. Castano, *CrystEngComm* **2015**, *17*, 1597–1602.
- [21] H.-Y. Dang, X.-M. Guo, *Sensors and Actuators B Chemical* **2013**, *178*, 163–168.
- [22] J. W. Fergus, *Journal of Solid State Electrochemistry* **2011**, *15*, 971–984.
- [23] N.-J. Choi, H.-K. Lee, S. E. Moon, W. S. Yang, J. Kim, *Sensors and Actuators B Chemical* **2013**, *187*, 340–346.
- [24] L. Wang, R. V. Kumar, *Sensors and Actuators B Chemical* **2003**, *88*, 292–299.
- [25] T. Kida, Y. Miyachi, K. Shimano, N. Yamazoe, *Sensors and Actuators B Chemical* **2001**, *80*, 28–32.
- [26] K. Kaneyasu, K. Otsuka, Y. Setoguchi, S. Sonoda, T. Nakahara, I. Aso, N. Nakagaichi, *Sensors and Actuators B Chemical* **2000**, *66*, 56–58.

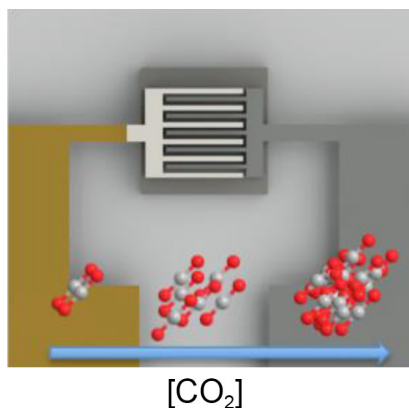
Received: May 24, 2017

Accepted: July 6, 2017

Published online on ■■■■■, 0000

FULL PAPER

Wide range CO₂ sensor: Exploiting microelectronics and nanotechnology a potentiometric thin-film sensor of 300 nm is designed and fabricated for monitoring CO₂ concentrations from 2 to 100 % at 450 °C (see picture). The sensor has a stable and reproducible response to CO₂ in a wide range of concentrations. Moreover the recovery time, stability, repeatability and selectivity of the sensor proves the feasibility of the use of this system for biogas and natural gas applications.



*Dr. L. Rojo, Dr. I. Castro-Hurtado,
G. G. Mandayo, E. Castaño,
Dr. M. C. Morant-Miñana**

1 – 8

**Thin-Film Potentiometric Sensor to
Detect CO₂ Concentrations
Ranging Between 2 % and 100 %**

